Progress In Electromagnetics Research, PIER 62, 165–192, 2006

ON THE DESIGN OF PATCH ANTENNAS TUNED BY TRANSVERSELY MAGNETIZED LOSSY FERRITE INCLUDING A NOVEL RESONATING MODE

A. A. Mavridis and G. A. Kyriacou

Department of Electrical and Computer Engineering
Democritus University of Thrace
GR-67100, Xanthi, Greece

J. N. Sahalos

Department of Physics
Aristotle University of Thessaloniki
GR-54066, Thessaloniki, Greece

Abstract—Circularly symmetric patch antennas tuned by transversely magnetized lossy ferrite are studied. The circular and ring patch geometries printed on ferrite substrate or tuned by ferrite post and ferrite toroid are studied. Both saturated and partially magnetized ferrite are considered. Strong effects on the dispersive properties of modes propagating under the patch and in turn on the antenna resonant frequency and input impedance are observed when the ferrite losses are taken into account. The patch antennas resonance at a novel mode propagating in the traditionally assumed switch-off frequency range of negative effective permeability constitutes an essential original contribution of this work. In all cases the dynamic control of the patch resonant frequency through the DC-biasing field is investigated. The "perfect magnetic walls approximation" was employed in the analysis since it offers a valuable physical insight as well as simplified closed form expressions for the resonant conditions. These are used as engineering design formulas for an initial antenna design, which is in turn fine tuned with the aid of a numerical simulation-optimization scheme. The validity of the present method was verified through comparisons with published experimental results and numerical simulations.

1. INTRODUCTION

Antennas printed on magnetized substrates can offer beam steering even with a single element as well as the ability of electronic tuning. The high permittivity of ferrite material yields a significant miniaturization of the antennas. The DC magnetization of the ferrite constitutes the most difficult task in the development of these antennas. Miniaturized electromagnets e.g., [1] along with the employment of ferrite posts or ferrite films are very promising solutions to overcome this difficulty.

A circular patch antenna tuned by a ferrite post was studied in our previous work [2]. A very strange phenomenon concerning the antenna tuneability was observed when the ferrite losses were ignored. Namely a fictitious increase in tuneability was observed when the ferrite post diameter was reduced, while the opposite was expected. This phenomenon was more intense when the patch resonant frequency was approaching the asymptotes of the negative effective permeability range. However, all these curious observations disappear when the ferrite losses were included in the analysis. Also, as the frequency tends to the asymptotes of the negative effective permeability μ_{eff} the permeability μ tends to infinity, if ferrite losses are ignored. This enables the existence of an infinite number of modes. However this is just theoretical, since when losses are taken into account μ becomes finite and the number of modes is drastically reduced, even for very small damping factors.

It was traditionally assumed that there is not any propagating mode in the substrate below the patch radiator for the area where μ_{eff} is negative. This was based on the obvious fact that the corresponding wavenumber becomes imaginary leading to an evanescent mode which disappears at a small distance from the feeding point. It was thus considered by many authors, e.g., [3], that this is a cutoff state and if the ferrite substrate is biased in region $\mu_{eff} < 0$ the antenna would not resonate. However when we included losses in the characteristic equation, even when the damping factor is assumed very small (e.g., a ferrite linewidth of the order of ΔH$\approx 10^{-4}$), a single propagating mode occurred within the assumed cutoff area of negative μ_{eff}. This mode is studied herein as well and it was found that the antenna is indeed resonating at this mode, which is Left Hand Circularly Polarized (LHCP). This important result is also verified by accurate numerical simulations using commercially available software. To the authors knowledge there isn't any published work presenting this phenomenon for antenna printed on ferrite substrate. A further study reveals that this LHCP mode behaves like the natural circularly polarized

mode of ferrites which occurs for DC-bias $\overline{H}_{DC} = H_0\widehat{z}$ along the propagation direction, although in the present case resonance occurs due to propagation transverse to the DC-bias. In view of this, the LHCP natural modes depend on the quantity $\mu^- = \mu - \kappa$ which is positive in the region of $\mu_{eff} < 0$. It is also observed that reversing the DC bias as $\overline{H}_{DC} = -H_0\widehat{z}$, the quantity $\mu^+ = \mu + \kappa$ becomes positive and $\mu^- < 0$ in the region $\mu_{eff} < 0$. In turn the Right Hand Circularly Polarized (RHCP) becomes propagating and LHCP evanescent in the region $\mu_{eff} < 0$. Finally, it was verified that these observations are indeed true even when losses are ignored, provided that the numerical problems involved in the calculation of Bessel functions are properly handled. A very convenient way to avoid these numerical problems is to introduce some negligible losses, e.g., ΔH$\approx 10^{-4}$ and use subroutines for Bessel functions with complex arguments.

Searching the published literature we found only one similar work studying the mode spectrum propagating in a grounded ferrite substrate, [4]. Baccarelli et al. [4] have considered a lossy ferrite substrate biased with an H_{DC} parallel to the ground plane. Assuming propagation along the substrate, but in a direction transverse to the H_{DC}, they indeed found a single mode denoted as TE_{1+} in the region of negative μ_{eff}.

A detailed study to be presented below, shows that the above referred LHCP mode exists for all circularly symmetric patch antennas e.g., ring shaped, as well as in the case when only a ferrite post is used to tune the antenna. We expect that this phenomenon is independent of the patch shape and it will be present whenever the bias is transverse to the wave propagation direction. We are currently working toward this direction as well as the theoretical foundation of these novel modes and more results will be presented in follow up works. It is also of interest to note that the single resonating mode in the negative μ_{eff} region could be exploited in applications where a pure circularly polarized radiation is desired. Summarizing, the originality of the present method mainly concerns the novel single resonating mode in the region of negative μ_{eff} and the account for both ferrite and dielectric losses in this analysis. The latter clarifies which resonating modes are of practical importance.

In the following section the analysis of circular and ring patch antennas printed on a bulk ferrite substrate is first reviewed, while in turn their tuning by a ferrite post and ferrite toroid, are examined. Approximate engineering formulas and design curves will be presented for the antenna resonance characteristics. Since, patch antennas operate at resonance, their resonant dimensions are important for their design.

2. THEORETICAL ANALYSIS

The analysis starts from the circular and ring patch antenna printed on a bulk ferrite substrate. In order to minimize the ferrite material dimensions two alternative geometries are in turn studied: the circular patch tuned by a ferrite post and the circular or ring patch tuned by a ferrite toroid. In these cases the ferrite occupies only a part of the space under the patch, while the remaining is filled by a dielectric material. Closed form expressions are obtained for the resonant frequency in all cases. Concerning the ferrite permeability tensor, two cases are investigated: the saturated ferrite state which is valid for most practical applications and the partially magnetized ferrite state. The latter was mostly considered in order to justify the method with respect to measurements available in the literature.

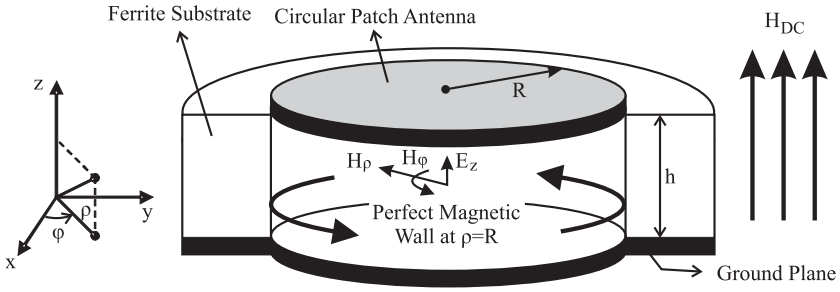

Figure 1. Geometry of circular patch antenna printed on magnetised ferrite substrate and perfect magnetic wall approximation.

2.1. Circular Patch Antenna Printed on Ferrite Substrate

The circular patch antenna printed on a transversely magnetized ferrite substrate ($\overline{H}_{DC} = H_0\hat{z}$), is shown in Fig. 1 The permeability tensor of a lossy saturated transversely magnetized ferrite is given by, [5]:

$$\bar{\bar{\mu}} = \begin{pmatrix} \mu_F & j\kappa_F & 0 \\ -j\kappa_F & \mu_F & 0 \\ 0 & 0 & \mu_0 \end{pmatrix} \tag{1}$$

where:

$$\mu_F = \mu_0 \cdot \left(1 + \frac{\omega_m(\omega_0 + j\alpha_F\omega)}{(\omega_0 + j\alpha_F\omega)^2 - \omega^2}\right) \tag{2}$$

and

$$\kappa_F = \mu_0 \frac{\omega \cdot \omega_m}{(\omega_0 + j\alpha_F\omega)^2 - \omega^2} \tag{3}$$

Also, γ is the gyromagnetic ratio, H_0 the DC biasing magnetic field, M_s the saturation magnetization and $\alpha_F = \frac{\mu_0 \gamma \Delta H}{2\omega_0}$ the damping factor [6], where ΔH is the ferrite linewidth. The subscript F refers to the ferrite and $\omega_0 = \mu_0 \gamma H_0$ and $\omega_m = \mu_0 \gamma M_s$.

The analysis begins with the determination of the field components below the circular patch. The ferrite substrate is considered electrically thin ($k_0 h = 2\pi h/\lambda_0 \ll 1$) and the same is assumed throughout this paper. In turn, field variations perpendicular to the substrate can be neglected $\partial/\partial z \approx 0$. The field wave equations along with their general solutions are given in classical textbook on ferrites, e.g., Lewin, [7]. The circular patch analysis using the "perfect magnetic wall PMW" approximation was presented in detail in our previous work [8]. This is summarized herein, in order to preserve a unified notation for all patch antennas to be studied. Only three components of the electromagnetic field exist under the patch and they are given by the following equations:

$$E_z = A^{\pm} \cdot J_n\left(K_{cF}\rho\right) \cdot e^{-jn\varphi} \tag{4}$$

$$H_\rho = A^{\pm} \cdot \frac{1}{\omega\mu_{eff}} \left\{ \frac{n}{\rho} J_n\left(K_{cF}\rho\right) - \frac{\kappa_F}{\mu_F} \cdot K_{cF} \cdot J_n'\left(K_{cF}\rho\right) \right\} \cdot e^{-jn\varphi} \tag{5}$$

$$H_\varphi = A^{\pm} \frac{1}{\omega\mu_{eff}} \left\{ -jK_{cF} J_n'\left(K_{cF}\rho\right) + j\frac{\kappa_F}{\mu_F} \cdot \frac{n}{\rho} J_n\left(K_{cF}\rho\right) \right\} \cdot e^{-jn\varphi} \tag{6}$$

where:

$$\mu_{eff} = \frac{\mu_F^2 - \kappa_F^2}{\mu_F}, \quad K_{cF}^2 = \omega^2 \epsilon_F \mu_{eff},\ n = 0, \pm 1, \pm 2, \ldots \tag{7}$$

κ_F, μ_F given in (2), J_n represents the nth order Bessel functions and the prime (J_n') denotes derivative with respect to its argument. The permittivity ϵ_F of the ferrite is considered complex in order to account for the ferrite dielectric losses: $\epsilon_F = \epsilon_0 \epsilon_{rF}\left(1 - j\tan\delta_F\right)$.

Applying the perfect magnetic wall boundary condition at the patch edge $\rho = R$ (Fig. 1), namely $H_\varphi|_{\rho=R} = 0$, the characteristic equation for the resonant frequency is obtained for the right (RHCP) and the left (LHCP) hand circular polarization as:

$$K_{cF}R \cdot \frac{J_n'(K_{cF}R)}{J_n(K_{cF}R)} - n\frac{\kappa_F}{\mu_F} = 0 \tag{8}$$

where $n = +1, +2, \ldots$ corresponds to the RHCP and $n = -1, -2, \ldots$ to the LHCP modes. Note that all quantities involved in equation (8) are complex since losses are taken into account. However the

resonant condition is determined by constructive interference of waves emanating from the probe and reflected from the perfect magnetic walls at $\rho = R$. Namely, the resonant condition is defined by the phase of these waves, which in turn corresponds to the real part of equation (8). So, to estimate the resonance frequency, complex arithmetic should be used in equation (8) but then its real part is enforced to equal zero, yielding the resonant frequency.

It is important to study the relatively simple characteristic equation (8) when losses are included and when ignored. For the lossless case μ_{eff} becomes negative in the frequency range defined by $\mu_F = 0$ and $\mu_F^2 - \kappa_F^2 = 0$ or $\mu_F = -\kappa_F$, since $\mu_F = \kappa_F$ gives a negative root for frequency. It is:

$$\mu_F = 0 \leftrightarrow \omega = \omega_L = [\omega_0 (\omega_0 + \omega_m)]^{1/2} \text{ or } f_L = [f_0 (f_0 + f_m)]^{1/2} \quad (9)$$

$$\mu_F = -\kappa_F \leftrightarrow \omega = \omega_u = \omega_0 + \omega_m \quad \text{or} \quad f_u = f_0 + f_m \quad (10)$$

and $\mu_{eff} < 0$ for the range $f_L < f < f_u$.

Examining equation (8) for the lossless case (when all quantities are real) it is obvious that when $\mu_{eff} < 0$ then the antenna will not resonate, since a propagating wave requires a positive real part of K_{cF}^2 according to Waldron [9] or Pozar [6]. However, solving equation (8) including the ferrite losses (even when an arbitrarily small damping factor is considered e.g., $\Delta H \approx 10^{-4}$), a single LHCP $n = -1$ resonating mode is found in the area $\mu_{eff} < 0$. This is also verified by simulations with commercially available electromagnetic simulators. A concrete theoretical explanation of this important phenomenon is outside the scope of the present work (it will be given in a follow-up paper), but the basic idea is as follows. The PMW boundary condition at $\rho = R$ give rise to right (RHCP) and left (LHCP) hand circularly polarized (CP) waves. Even though hidden in the above analysis, these waves behave similar to the ferrite natural circularly polarized modes which occur when the ferrite is biased along the direction of propagation. These natural CP waves have wavenumbers proportional to RHCP: $K_c^+ = \omega\sqrt{\epsilon\mu^+}$ and LHCP: $K_c^- = \omega\sqrt{\epsilon\mu^-}$ where $\mu^+ = \mu_F + \kappa_F$, $\mu^- = \mu_F - \kappa_F$. From a different point of view the field below the patch can be expressed as a superposition of these natural CP waves.

The gyromagnetic resonance frequency f_0 along with f_L and f_u define four different ranges where the ferrite quantities μ_F, κ_F and those depending on them μ^-, μ^+, μ_{eff} and κ_F/μ_F may change sign. Their signs for a biasing field along the positive z-axis ($\overline{H}_{DC} = H_0\hat{z}$) are shown in Table 1, while for a reversed bias ($\overline{H}_{DC} = -H_0\hat{z}$) these signs are presented in Table 2. Note, that when the bias is reversed

Table 1. Signs of ferrite permeability characteristics in the regions defined by f_0, f_L and f_u for positive bias $\overline{H}_{DC} = +H_0\widehat{z}$.

Frequency	$\rightarrow$	f_0	$\rightarrow$	f_L	$\rightarrow$	f_u	$\rightarrow$
μ_F	+	∞	-	0	+	|	+
κ_F	+	∞	-	|	-	|	-
$\mu^- = \mu_F - \kappa_F$	+	|	+	|	+	|	+
$\mu^+ = \mu_F + \kappa_F$	+	∞	-	|	-	0	+
$\mu_{eff} = \frac{(\mu_F - \kappa_F)(\mu_F + \kappa_F)}{\mu_F^2}$	+	|	+	∞	-	0	+
κ_F/μ_F	+	|	+	∞	-	|	-

Table 2. Signs of ferrite permeability characteristics in the regions defined by f_0, f_L and f_u for reversed bias $\overline{H}_{DC} = -H_0\widehat{z}$.

Frequency	$\rightarrow$	f_0	$\rightarrow$	f_L	$\rightarrow$	f_u	$\rightarrow$
μ_F	+	∞	-	0	+	|	+
κ_F	-	∞	+	|	+	|	+
$\mu^- = \mu_F - \kappa_F$	+	∞	-	|	-	0	+
$\mu^+ = \mu_F + \kappa_F$	+	|	+	|	+	|	+
$\mu_{eff} = \frac{(\mu_F - \kappa_F)(\mu_F + \kappa_F)}{\mu_F^2}$	+	|	+	∞	-	0	+
κ_F/μ_F	-	|	-	∞	+	|	+

both H_{DC} and M_s will change signs causing a change in the sign of ω_0 and ω_m. In turn from expressions (2) the sign of κ_F will change while that of μ_F will remain unchanged.

Observing Table 1, it can be seen that in the range of $\mu_{eff} < 0$ it is $\mu^+ < 0$ but $\mu^- > 0$. Thus RHCP modes will be at cut-off while LHCP mode will propagate yielding a patch resonance. In contrary, when the bias is reversed (Table 2) it is $\mu^+ > 0$ but $\mu^- < 0$ in the range of $\mu_{eff} < 0$, as can be seen from Table 2, causing LHCP to be at cut-off and RHCP to propagate. These phenomena will be presented solving equation (8) and verified by numerical electromagnetic simulations. Moreover, similar phenomena are observed in the analysis of patch antennas studied in the next sections.

2.1.1. Partially Magnetized Ferrite

The classical ferrite permeability tensor given in equation (1) is valid only when the ferrite is saturated, which is the usual practice, since operating the ferrite at saturation minimizes its losses. Comparing the results of equation (8) with experimental results presented in [10] and [11], the expected totally different behaviour of the resonant frequency curves was observed, for values of DC biasing field H_0 corresponding to magnetization M well below saturation $4\pi M < 4\pi M_s$. In order for the above approximate theory to describe the partial ferrite magnetization, the appropriate permeability tensor is incorporated. The partially magnetized ferrite state was studied by many authors, e.g., Green and Sandy [12] and the permeability tensor they proposed was:

$$\bar{\bar{\mu}} = \begin{pmatrix} \mu & -j\kappa & 0 \\ j\kappa & \mu & 0 \\ 0 & 0 & \mu_z \end{pmatrix} \tag{11}$$

where:

$$\begin{cases} \mu = \mu' - j\mu'' \\ \kappa = \kappa' - j\kappa'' \\ \mu_z = \mu'_z - j\mu''_z \end{cases}, \quad \mu' = \mu'_0 + (1 - \mu'_0) \cdot \left(\frac{M}{M_s}\right)^{3/2}, \quad \kappa' = \gamma 4\pi M/\omega \tag{12}$$

μ'_0 corresponds to the completely unmagnetized state and it is given by:

$$\mu'_0 = \frac{2}{3} \cdot \left[1 - \left(\frac{\gamma 4\pi M_s}{\omega}\right)^2\right]^{1/2} + \frac{1}{3} \tag{13}$$

Employing the above magnetic permeability tensor, in the characteristic equation (8) the calculated resonant frequency was in a satisfactory agreement with measured results given in the literature, but only for partial magnetization $M < M_s$. For the saturated state $M \geq M_s$ the classical permeability tensor of Eq. (1) was always found to operate satisfactorily.

2.1.2. Circular Patch Radiation Pattern

The far field of the circular patch geometry is then studied, through the magnetic current density on the patch edge at $\rho = R$. The detailed study was presented in our previous work [13] and the final expressions for the far field are:

$$\begin{aligned} E_\varphi \;=\; & (j)^{n+1} \frac{A^{\pm} R k_0 h}{2} \cdot \frac{e^{-jk_0 r}}{r} \cdot J_n\left(K_{cF} R\right) \cdot \cos\theta \\ & \cdot \left[J_{n+1}\left(k_0 R \sin\theta\right) + J_{n-1}\left(k_0 R \sin\theta\right)\right] \cdot e^{-jn\varphi} \end{aligned} \tag{14}$$

$$E_\theta = -(j)^n \frac{A^{\pm} R k_0 h}{2} \cdot \frac{e^{-jk_0 r}}{r} \cdot J_n(K_{cF} R) \cdot [J_{n+1}(k_0 R \sin\theta) - J_{n-1}(k_0 R \sin\theta)] \cdot e^{-jn\varphi} \quad (15)$$

Expressions (14) and (15) show that their angular terms are independent from the ferrite permeability. Namely, there is not any radiation pattern control for transverse ferrite bias. This is basically expected to occur only in the case when the biasing field is oriented parallel to the substrate and normal to the propagation direction.

2.2. Ring Patch Antenna Printed on Ferrite Substrate

The geometry of the ring patch antenna ($\alpha \leq \rho \leq b$) printed on a magnetized ferrite substrate is shown in Fig. 2. From a first point of view the ferrite substrate material could cover the whole area from $\rho = 0$ to $\rho = b$. However, this could be restricted only under the ring, leaving the rest of the area ($\rho < \alpha$ and $\rho > b$) empty or filled by another dielectric material. This is an important advantage of the ring geometry. In any case, the perfect magnetic wall approximation employed herein, cannot account for the substrate material beyond the edges at $\rho = \alpha, b$.

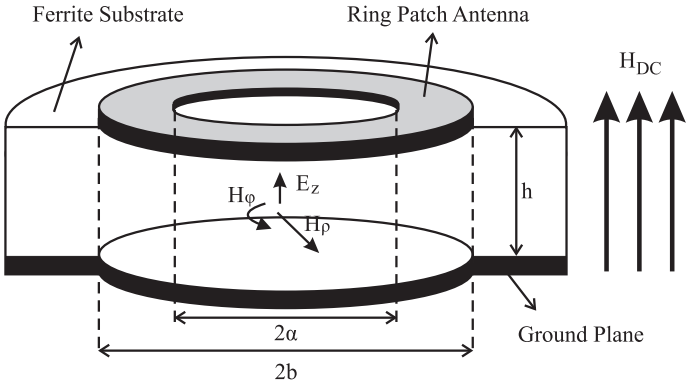

Figure 2. Ring patch antenna printed on magnetized ferrite substrate.

The procedure is similar to that of the circular patch antenna, with the only difference that the general solution of the field underneath the patch includes the Newman functions (Y_n):

$$E_z = A^{\pm} \{J_n(K_{cF}\rho) - f^n(K_{cF}\alpha) \cdot Y_n(K_{cF}\rho)\} \cdot e^{-jn\varphi} \quad (16)$$

where:

$$f^n(K_{cF}\alpha) = \frac{\frac{\kappa_F}{\mu_F}\cdot\frac{n}{\alpha}\cdot J_n(K_{cF}\alpha) + K_{cF}\cdot J_n'(K_{cF}\alpha)}{\frac{\kappa_F}{\mu_F}\cdot\frac{n}{\alpha}\cdot Y_n(K_{cF}\alpha) + K_{cF}\cdot Y_n'(K_{cF}\alpha)} \tag{17}$$

$$\begin{aligned} H_\rho &= A^{\pm}\frac{1}{\omega\mu_{eff}}\left\{K_{cF}\left[J_n'(K_{cF}\rho) - f^n(K_{cF}\alpha)\cdot Y_n'(K_{cF}\rho)\right]\right. \\ &\quad \left. + \frac{n}{\rho}\left[\frac{\kappa_F}{\mu_F}\cdot J_n(K_{cF}\rho) - f^n(K_{cF}\alpha)\cdot Y_n(K_{cF}\rho)\right]\right\} e^{-jn\varphi} \end{aligned} \tag{18}$$

$$\begin{aligned} H_\varphi &= A^{\pm}\frac{-j}{\omega\mu_{eff}}\left\{\frac{\kappa_F}{\mu_F}\cdot\frac{n}{\rho}\left[J_n(K_{cF}\rho) - f^n(K_{cF}\alpha)\cdot Y_n(K_{cF}\rho)\right]\right. \\ &\quad \left. + K_{cF}\left[J_n'(K_{cF}\rho) - f^n(K_{cF}\alpha)\cdot Y_n'(K_{cF}\rho)\right]\right\} e^{-jn\varphi} \end{aligned} \tag{19}$$

The boundary conditions now are imposed at the edges $\rho = \alpha \rightarrow H_\varphi|_{\rho=\alpha} = 0$ and $\rho = b \rightarrow H_\varphi|_{\rho=b} = 0$ and the resulting characteristic equation reads:

$$\frac{\frac{\kappa_F}{\mu_F}\cdot\frac{n}{\alpha}\cdot J_n(K_{cF}\alpha) + K_{cF}J_n'(K_{cF}\alpha)}{\frac{\kappa_F}{\mu_F}\cdot\frac{n}{\alpha}\cdot Y_n(K_{cF}\alpha) + K_{cF}Y_n'(K_{cF}\alpha)} = \frac{\frac{\kappa_F}{\mu_F}\cdot\frac{n}{b}\cdot J_n(K_{cF}b) + K_{cF}J_n'(K_{cF}b)}{\frac{\kappa_F}{\mu_F}\cdot\frac{n}{b}\cdot Y_n(K_{cF}b) + K_{cF}Y_n'(K_{cF}b)} \tag{20}$$

where $n = +1, +2, \ldots$ corresponds to the RHCP and $n = -1, -2, \ldots$ to the LHCP.

2.2.1. Ring Patch Radiation Pattern

The far field of this geometry is once again found by determining the electric vector potential from the equivalent magnetic current density along the two edges ($\rho = \alpha$ and $\rho = b$). The final expressions take the form:

$$\begin{aligned} E_\varphi = &-(j)^{n+1}\cdot n\cdot A^{\pm}\cdot h\cdot\frac{e^{-jk_0r}}{r}\cdot\frac{\cos\theta}{\sin\theta} \\ &\cdot\left\{M_{\varphi'}(K_{cF}\alpha)\,J_n(k_0\alpha\sin\theta) - M_{\varphi'}(K_{cF}b)\,J_n(k_0b\sin\theta)\right\}\cdot e^{-jn\varphi} \end{aligned} \tag{21}$$

$$\begin{aligned} E_\theta &= -(j)^n\cdot A^{\pm}\cdot k_0h\cdot\frac{e^{-jk_0r}}{r}\cdot\left\{\alpha\cdot M_{\varphi'}(K_{cF}\alpha)\cdot J_n'(k_0\alpha\sin\theta)\right. \\ &\quad \left. - b\cdot M_{\varphi'}(K_{cF}b)\cdot J_n'(k_0b\sin\theta)\right\}\cdot e^{-jn\varphi} \end{aligned} \tag{22}$$

where:

$$M_{\varphi'}(K_{cF}w) = J_n(K_{cF}w) - f^n(K_{cF}w)\cdot Y_n(K_{cF}w) \tag{23}$$

for $w = \alpha, b$ and (ρ', φ', z') corresponds to the cylindrical while (r, θ, φ) to the spherical coordinate system.

2.3. Circular Patch Antenna tuned by Ferrite Post

The main idea here is the reduction of the ferrite using only a ferrite post for tuning. The benefit from such a design is the reduction of losses and weight. The critical point here is to minimize the ferrite material dimensions and at the same time retain the electronic tuning and the other features offered by the ferrite substrate. Another consideration was whether to place the ferrite post at the centre which is simpler to analyze, or to shift it to an offset location which offers more degrees of freedom (e.g., multiple posts). The latter requires a coordinate transformation and it is also under consideration. Moreover, for a single post the central location is preferable as it preserves a strong interaction with the magnetic field.

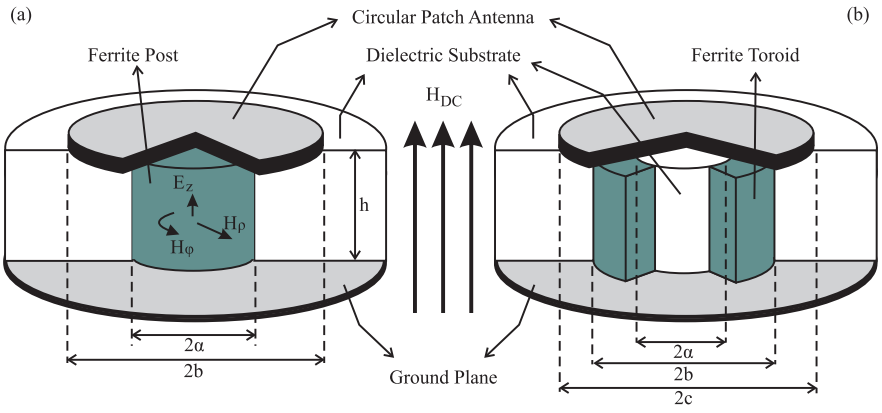

Figure 3. Geometry of a circular patch antenna tuned by transversely magnetized ferrite (a) post and (b) toroid.

The detailed analysis was performed in our previous work [2]. Herein we only include the characteristic equation in order for this to be re-examined in view of the novel resonance in the negative μ_{eff} range. This takes the form:

$$\frac{1}{\mu_{eff}} \cdot \left\{ K_{cF} \frac{J_n'(K_{cF}\alpha)}{J_n(K_{cF}\alpha)} - \frac{\kappa_F}{\mu_F} \cdot \frac{n}{\alpha} \right\} = \frac{k_{cD}}{\mu_D} \left\{ \frac{J_n'(k_{cD}\alpha) \cdot Y_n'(k_{cD}b) - Y_n'(k_{cD}\alpha) \cdot J_n'(k_{cD}b)}{J_n(k_{cD}\alpha) \cdot Y_n'(k_{cD}b) - Y_n(k_{cD}\alpha) \cdot J_n'(k_{cD}b)} \right\} \quad (24)$$

where n=+1,+2,... corresponds to the RHCP, while n=-1,-2,... to the LHCP. $k_{cD}^2 = \omega^2 \mu_{rD} \cdot \epsilon_{rD} (1 - j \tan \delta_\varepsilon)$ and subscript D refers to the dielectric substrate. The permittivity is considered complex in order to account for the dielectric losses.

2.4. Circular Patch Antenna tuned by Ferrite Toroid

A circular patch antenna tuned by a ferrite toroid is shown in Fig. 3(b). The ferrite material covers the area under the patch of radius c, from radius α to radius b ($\alpha < b < c$), while a dielectric material covers the rest of the area ($0 \leq \rho \leq \alpha$, $\rho \geq b$). In general, different dielectric materials can be used for the two areas $0 \leq \rho \leq \alpha$ (ϵ_1, μ_1) and $\rho \geq b$ (ϵ_2, μ_2).

The field components under the patch are defined first, separately for each material: inner dielectric, ferrite toroid and outer dielectric. The assumptions are the same as in the previous geometries and some preliminary analytical results were presented in a previous conference paper [13]. The field expressions read:
Inner dielectric region ($0 \leq \rho \leq \alpha$):

$$E_{z1} = A_1 \cdot J_n (k_{c1}\rho)\, e^{-jn\varphi} \tag{25}$$

$$H_{\rho 1} = A_1 \cdot \frac{n}{\omega \mu_1} \cdot \frac{J_n (k_{c1}\rho)}{\rho} e^{-jn\varphi} \tag{26}$$

$$H_{\varphi 1} = -A_1 \cdot \frac{j}{\omega \mu_1} \cdot k_{c1} \cdot J_n' (k_{c1}\rho)\, e^{-jn\varphi} \tag{27}$$

Ferrite Region ($\alpha \leq \rho \leq b$):

$$E_{zF} = \left\{ A_F^{\pm} \cdot J_n (K_{cF}\rho) + B_F^{\pm} \cdot Y_n (K_{cF}\rho) \right\} e^{-jn\varphi} \tag{28}$$

$$H_{\rho F} = \frac{1}{\omega \mu_{eff}} \left\{ \frac{\kappa_F}{\mu_F} \cdot K_{cF} \left[A_F^{\pm} \cdot J_n' (K_{cF}\rho) + B_F^{\pm} \cdot Y_n' (K_{cF}\rho) \right] + \frac{n}{\rho} \left[A_F^{\pm} \cdot J_n (K_{cF}\rho) + B_F^{\pm} \cdot Y_n (K_{cF}\rho) \right] \right\} e^{-jn\varphi} \tag{29}$$

$$H_{\varphi F} = \frac{-j}{\omega \mu_{eff}} \left\{ \frac{\kappa_F}{\mu_F} \cdot \frac{n}{\rho} \left[A_F^{\pm} \cdot J_n (K_{cF}\rho) + B_F^{\pm} \cdot Y_n (K_{cF}\rho) \right] + K_{cF} \left[A_F^{\pm} \cdot J_n' (K_{cF}\rho) + B_F^{\pm} \cdot Y_n' (K_{cF}\rho) \right] \right\} e^{-jn\varphi} \tag{30}$$

Outer dielectric region ($b \leq \rho \leq c$):

$$E_{z2} = \{ A_2 \cdot J_n (k_{c2}\rho) + B_2 \cdot Y_n (k_{c2}\rho) \}\, e^{-jn\varphi} \tag{31}$$

$$H_{\rho 2} = \frac{n}{\omega \mu_2} \cdot \frac{1}{\rho} \{ A_2 \cdot J_n (k_{c2}\rho) + B_2 \cdot Y_n (k_{c2}\rho) \}\, e^{-jn\varphi} \tag{32}$$

$$H_{\varphi 2} = \frac{-j}{\omega\mu_2} \cdot k_{c2} \left\{ A_2 \cdot J_n'\left(k_{c2}\rho\right) + B_2 \cdot Y_n'\left(k_{c2}\rho\right) \right\} e^{-jn\varphi} \qquad (33)$$

The boundary condition at the $\rho = c$ surface and the continuity conditions at the ferrite-dielectric interfaces $\rho = \alpha$ and $\rho = b$ are imposed, resulting in the following characteristic equation:

$$\frac{k_{c2}}{\mu_2} \cdot \frac{J_n'\left(k_{c2}b\right) \cdot Y_n'\left(k_{c2}c\right) - J_n'\left(k_{c2}c\right) \cdot Y_n'\left(k_{c2}b\right)}{J_n\left(k_{c2}b\right) \cdot Y_n'\left(k_{c2}c\right) - J_n'\left(k_{c2}c\right) \cdot Y_n\left(k_{c2}b\right)} = -\frac{1}{\mu_{eff}} \cdot \frac{\kappa_F}{\mu_F} \cdot \frac{n}{b} + \frac{1}{\mu_{eff}} \cdot K_{cF} \cdot \frac{J_n'\left(K_{cF}b\right) - X_1 \cdot Y_n'\left(K_{cF}b\right)}{J_n\left(K_{cF}b\right) - X_1 \cdot Y_n\left(K_{cF}b\right)} \qquad (34)$$

where:

$$X_1 = \frac{\left(-\frac{1}{\mu_{eff}} \cdot \frac{\kappa_F}{\mu_F} \cdot \frac{n}{\alpha} \cdot J_n\left(k_{c1}\alpha\right) \cdot J_n\left(K_{cF}\alpha\right) + K_{cF} \cdot J_n\left(k_{c1}\alpha\right) \cdot J_n'(K_{cF}\alpha) - \frac{k_{c1}}{\mu_1} J_n'(k_{c1}\alpha) \cdot J_n(K_{cF}\alpha) \right)}{\left(-\frac{1}{\mu_{eff}} \cdot \frac{\kappa_F}{\mu_F} \cdot \frac{n}{\alpha} \cdot J_n(k_{c1}\alpha) \cdot Y_n(K_{cF}\alpha) + K_{cF} \cdot J_n(k_{c1}\alpha) \cdot Y_n'(K_{cF}\alpha) - \frac{k_{c1}}{\mu_1} J_n'(k_{c1}\alpha) \cdot Y_n(K_{cF}\alpha) \right)}$$

and $k_{c1} = \omega\sqrt{\epsilon_1\mu_1}$, $k_{c2} = \omega\sqrt{\epsilon_2\mu_2}$.

3. DESIGN PROCEDURE

The purpose of the design procedure is the estimation of a tunable patch antenna covering the desired bandwidth of operation (f_{min} to f_{max}) preserving a constant and matched input impedance as far as possible. First, the ferrite substrate or post and its DC biasing are selected based on the desired normalized tuning bandwidth (f_{max}/f_{min}). In general the patch shape is mostly dictated by the required polarization of the radiated field. The patch shape is herein restricted to the shapes studied for which the natural-eigen modes, propagating between the patch and the ground plane, are circularly polarized. In turn, this yields circularly polarized radiated field.

Once the patch geometry is decided, the substrate material must be chosen. There is a variety of commercially available ferrite materials fabricated especially to be used as microwave substrates. Most materials have a dielectric constant ϵ_{rF} between 12 and 15 and consequently its effect on the bandwidth is quite similar. The most important criterion for the selection between different substrates is the saturation magnetization ($4\pi M_s$) which will affect the size of the electromagnet needed and the shapes and sizes in which the ferrite material is fabricated. Also, the ferrite with the lower losses (smaller linewidth) is preferable.

The patch antenna excitation is closely related to the required matching with the feeding transmission line. Herein, a probe feed is considered and when possible it is preferable to avoid the insertion of the probe through the ferrite for practical convenience. Due to space limitations we will not elaborate on the preferable wideband matching. However, the appropriate feed point offering matching at the mean frequency of operation will be sought.

In order to systemize the design the patch dimensions will be first estimated considering an "equivalent" dielectric substrate, namely $\epsilon_r = \epsilon_{reff}$ and $\mu_r = 1$ for an operation at the mean frequency $f_m = (f_{max} + f_{min})/2$. In turn the resonant dimensions for the mean frequency of operation will be calculated employing the "perfect magnetic wall" closed form expressions, along with some "corrections" proposed in the literature for patch antennas printed on a dielectric substrate. Then the patch dimensions are adapted to the ferrite tuned geometry using the expressions obtained from the analysis of the previous sections. These equations are solved numerically, but the whole procedure is quite fast since we have to deal with closed form expressions. Finally, a numerical simulation using commercially available software is carried out with twofold scope, to validate the design procedure, but more important to fine tune the geometry-dimensions when needed. In the following two subsections some important details for the design of the circular and ring patch shapes will be given.

3.1. Circular Patch Geometry

First, the appropriate radius of the circular patch must be defined. At first the ferrite substrate is considered as a dielectric material with $\epsilon_r = \epsilon_{rF}$ and $\mu_r = 1$ with a resonant frequency given approximately by [14]:

$$f_r = \frac{K_{nm}C}{2\pi a_{eff}\sqrt{\epsilon_r}} \tag{35}$$

where a_{eff} is the effective radius

$$a_{eff} = a\left[1 + \frac{2h}{\pi a \epsilon_r}\left(\ln\left(\frac{\pi a}{2h}\right) + 1.7726\right)\right]^{1/2} \tag{36}$$

h is the substrate height, α is the patch radius, K_{nm} is the mth zero of the derivative of the Bessel function of order n and C is the velocity of light. The resonant frequency (f_r) is considered equal to the central value of the frequency band of operation ($f_r = f_m$).

Next, the resonant dimensions of the patch must be corrected taking into account the ferrite characteristics with the aid of (8). The

initial value used for the patch radius is the one found from equations (35) and (36). A Fortran 90 code developed for this purpose. This evaluates the resonant frequency within a specified DC magnetization range, keeping the patch radius constant. Running the program iteratively, the patch radius is updated accordingly in order for the resonant frequency to tune over the desired bandwidth ($f_{min} - f_{max}$).

The ferrite material reduction must be considered at this point. There are two equations available depending on the shape of the ferrite that will be used. Equation (24) concerns the ferrite post and equation (35) the ferrite toroid tuned patch antenna. A very useful consideration here is the selection of the dielectric material that will cover the remaining area under the patch, since it can affect not only the resonant frequency of the antenna, but also its bandwidth. The bandwidth of the antenna can be improved by choosing a material with low dielectric constant (foam with $\epsilon_r = 1.1$). A Fortran 90 code has been developed for the two ferrite substrate geometries and starting from the radius estimated for the bulk ferrite substrate, the new patch radius is evaluated.

The final step is the fine tuning of the antenna using a commercially available numerical simulator. Following the above design procedure the final patch radius will be defined after only 2 or 3 simulations. After completing this task the antenna can be fabricated.

3.2. Ring Patch Geometry

The same procedure as in the circular patch geometry is followed as well, considering the ferrite substrate as a dielectric material with $\epsilon_r = \epsilon_{rF}$ and $\mu_r = 1$. The initial resonant dimensions α and b will result from the following equations [14]:

$$f_r = \frac{C}{2\pi\sqrt{\epsilon_{eff}}} \cdot \frac{2n}{\alpha + b} \tag{37}$$

where:

$$\epsilon_{eff} = \frac{\epsilon_r + 1}{2} + \frac{\epsilon_r - 1}{2}\left(1 + \frac{12h}{W}\right)^{-1/2} \tag{38}$$

The resonant frequency (f_r) is considered equal to the central value of the frequency band of operation, C is the velocity of light, h is the substrate height and $W = b - \alpha$. The resonant dimensions evaluated here, are then used as an initial value in the characteristic equation (20), where the ferrite characteristics are taken into account. A Fortran 90 code was developed to solve this equation and the patch dimensions are estimated in a way similar to the circular geometry. These are also fine tuned using a commercially available numerical simulator.

4. NUMERICAL RESULTS

A representative geometry for each case studied in the theoretical analysis section is presented. In most cases, the basic criterion was to design an antenna operating at a specific frequency band. However, in some cases where comparison with published experimental results was desired, the antenna given in the corresponding literature is adopted.

Three types of ferrites are used throughout this section. The first "Ferrite-1" is the YIG-Al doped type "GA-65" of Ferrite Domen with $4\pi M_s = 650$Gauss, $\epsilon_{rF} = 14.2$ and $\Delta H = 45$ Oe. The second "Ferrite-2" is used in [15] with $4\pi M_s = 650$Gauss and $\epsilon_{rF} = 9.35$. Because there is not any data given in [15] for the linewidth or the type of the ferrite, the linewidth ΔH is considered equal to 45 Oe throughout this section. The third "Ferrite-3" is the "TT2-2750" Nickel Ferrite of Trans-Tech with $4\pi M_s = 2750$Gauss, $\epsilon_{rF} = 12.6$ and $\Delta H = 540$ Oe. In the same way, two types of dielectrics are used: the RT/duroid 5870 with $\epsilon_{rD} = 2.33$ and $\tan\delta = 0.0022$ the ceramic-PTFE substrate TMM10 with $\epsilon_{rD} = 9.2$ and $\tan\delta = 0.0009$. Both dielectrics are fabricated by Rogers. Finally, the substrate thickness for all the geometries studied is $h = 0.8$ mm.

4.1. Results for a Circular Patch Antenna printed on Ferrite Substrate

The electronic tuning offered by the ferrite substrates is exploited for the design of a single antenna capable to operate in the range 800–2000 MHz. The "Ferrite-1" material is used as a substrate. Following the design procedure described in paragraph 3.1 the patch radius is found to be $R = 6$ mm. The resonant frequency versus the DC biasing field of this antenna is plotted in Fig. 4(a). The dashed area represents negative effective permeability $\mu_{eff} < 0$. This area is bounded by two dotted lines defined by the lower (f_L) and upper (f_u) limiting frequencies given in equations (9) and (10).

The most important observation that should be noted here is the behaviour of the second LHCP ($n = -1$) mode (denoted in red symbols). It is clear that this mode does not vanish when it reaches the upper negative μ_{eff} asymptote, but it continues to propagate inside the negative μ_{eff} region. This confirms the prediction made in Section 2.1. On the other hand, the first LHCP ($n = -1$) mode tends to coincide with the lower negative μ_{eff} asymptote, as the DC magnetization H_0 decreases. However, the mode vanishes below $H_0 = 100$ Oe. The same parametric investigation but for a reverse biased ferrite substrate ($\overline{H}_{DC} = -H_0\hat{z}$) is shown in Fig. 4(b). It is clear that the behaviour

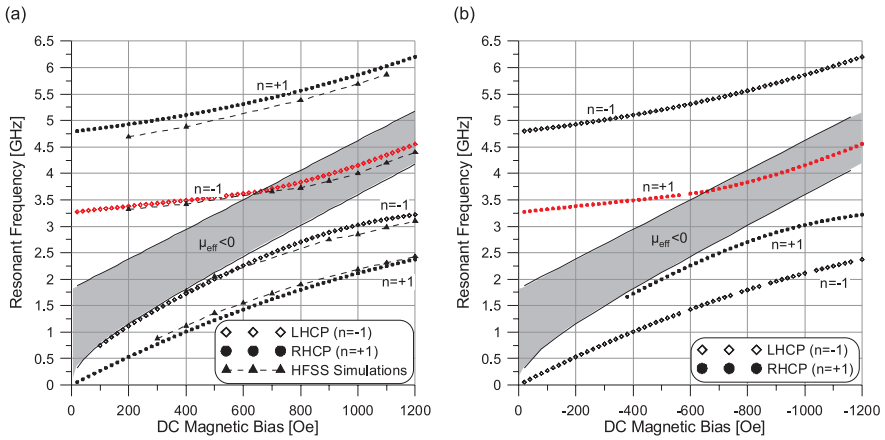

Figure 4. Resonant frequency of circular patch (R=6mm) printed on "Ferrite-1" type substrate versus DC magnetization (a) for positive $\overline{H}_{DC} = H_0\hat{z}$ and (b) for reverse $\overline{H}_{DC} = -H_0\hat{z}$ bias.

of RHCP ($n = +1$) and LHCP ($n = -1$) modes are now interchanged, with the RHCP $n = +1$ mode entering the $\mu_{eff} < 0$ region.

In order to confirm the validity of our results, a comparison against numerical simulations is also presented in Fig. 4(a). The software used was the Ansoft $HFSS^{©}$ 3D Electromagnetic Simulator [16], which is based on the finite element method. A convenient advantage of this software is its ability to account for the ferrite losses. The deviation between Perfect Magnetic Walls (PMW) and HFSS simulations for the dominant $n = +1$ RHCP and $n = -1$ LHCP modes is less than 5% at all frequency points. Moreover, the simulation results confirm the excitation of the second LHCP ($n = -1$) mode inside the negative μ_{eff} region.

The graph of Fig. 5 presents the resonant frequency of a circular patch antenna of radius $R = 10.1$ mm printed on a partially magnetized "Ferrite-2" type substrate. This specific geometry is the same as the one published by Araki et al. [15]. The dashed line with the triangular markers corresponds to measurements presented in [15], while the curves denoted by the circular and rhomb markers correspond to the calculations using the "Perfect magnetic walls" approximation. The maximum deviation between PMW and measurements is about 4%.

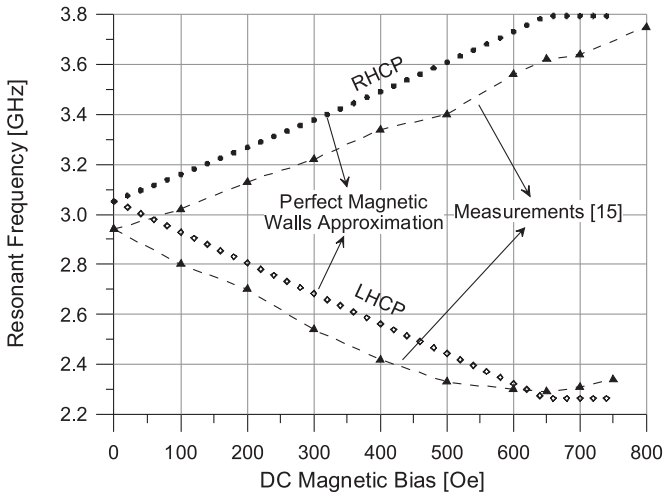

Figure 5. Resonant frequency of circular patch antenna printed on partially magnetized ferrite: comparison between PMW approximate calculations and measurements by Araki et al. [15].

4.2. Results for a Ring Patch Antenna printed on Ferrite Substrate

The resonant frequency of a ring patch antenna versus the DC magnetization field is presented in Fig. 6. The procedure of paragraph 3.2 was followed in order to design an antenna resonating in the 5.0 GHz to 5.5 GHz frequency band. The substrate used was the "Ferrite-2" type. The inner and outer patch radius resulted were $\alpha = 1.5$ mm and $b = 6$ mm. Curves for both the partially magnetized (black circles) and the saturated state (empty circles) of the ferrite are presented. The partially magnetized permeability tensor equations (11)–(13) are used for DC bias $H_0 < 4\pi M_s$, while for $H_0 > 4\pi M_s$ the saturated ferrite permeability tensor equations (1)–(3) are employed. A vertical dashed line at the point $H_0 = 4\pi M_s = 650$ Oe is drawn in order to indicate the change between the two models of the ferrite permeability tensor. It is observed that the $n = +1$ RHCP and $n = -1$ LHCP curves are not continuous at $H_0 = 4\pi M_s$ where the model changes from partially to saturated ferrite. But, still the deviation is small and reaches about 3.5% for the worst case which appears at the LHCP mode curve. The results marked with empty circles show that the saturated ferrite model is invalid for $H_0 < 4\pi M_s$, especially for the LHCP $n = -1$ mode.

Fig. 6 also presents a comparison of "Perfect magnetic walls"

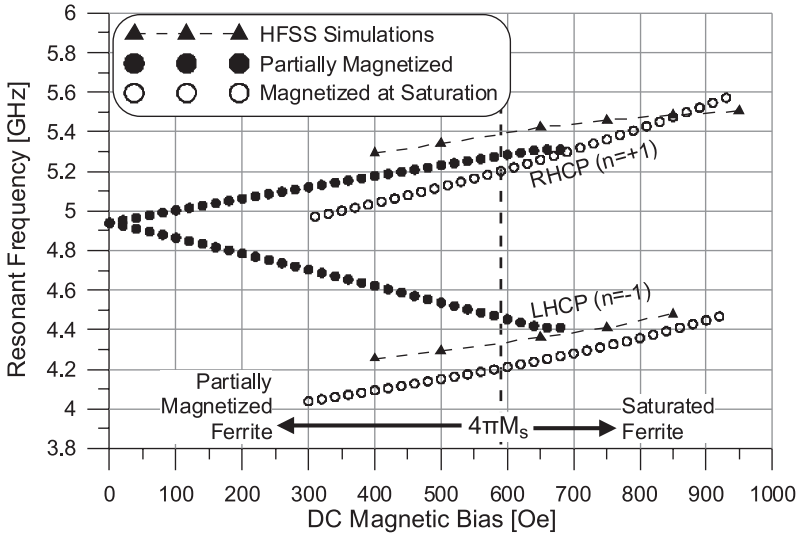

Figure 6. Resonant frequency of ring patch antenna ($\alpha = 1.5\,\text{mm}$, $b = 6\,\text{mm}$) printed on "Ferrite-2" substrate versus DC magnetization.

approximation against results from Ansoft $HFSS^{©}$ simulations. The comparison is valid only for the saturated ferrite state, since the saturated permeability tensor is used within this software. The agreement is yet again satisfactory reaching 3% deviation in the worst case.

4.3. Results of a Circular Patch Antenna tuned by a Ferrite Post

The choice of the ferrite to dielectric (α/b) ratio is a very critical parameter here since the reduction of ferrite material leads to a degradation of the tuning sensitivity of the antenna. The subject was extensively investigated in our previous work [2] where a ratio of $\alpha/b \approx 0.3$ was found to be a good compromise between ferrite material reduction and electronic tuning.

In the present example a $\alpha/b = 0.5$ ratio is chosen in order to preserve a quite strong tuning sensitivity. The substrate materials consist of "Ferrite-1" (ferrite post) and "TMM10" (dielectric). The antenna was designed to resonate at the 2.4 GHz frequency band, which resulted to a radius of $b = 7.5\,\text{mm}$. The resonant curves of the antenna against DC magnetization along with a comparison against Ansoft $HFSS^{©}$ [16] numerical simulations are shown in Fig. 7. The

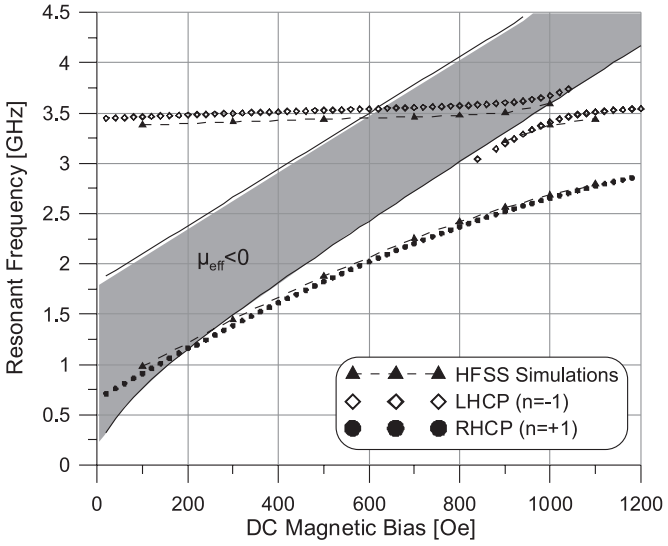

Figure 7. Dominant LHCP $n = -1$ and RHCP $n = +1$ resonant frequencies versus DC magnetization with "Ferrite-1" and a dielectric "TMM10" materials for the substrate, $\alpha/b = 0.5$ and $b = 7.5\,\text{mm}$.

excitation of the second LHCP ($n = -1$) mode inside the negative μ_{eff} region can be clearly observed and this is also confirmed by the HFSS simulations. On the other hand the lower LHCP mode vanishes at $H_0 = 900\,\text{Oe}$ as the DC magnetization decreases. A strange behaviour is observed for the RHCP ($n = +1$) mode curve, which enters the negative μ_{eff} region as the DC magnetization decreases. This result is also confirmed by an HFSS simulation performed for DC magnetic bias $H_0 = 100\,\text{Oe}$ which shows a resonance at 0.97 GHz. Note that the ferrite constitutes only a post in this case and a further understanding of this phenomenon is required.

Compared to the HFSS simulations, the "PMW approximation" results prove to be quite accurate, since there is only a 3% deviation in the worst case. Finally, it should be noted that a ratio of $\alpha/b = 0.5$ is significant since it corresponds to a ferrite material volume of 25% compared to the total volume under the patch.

4.4. Results of a Circular Patch Antenna tuned by Ferrite Toroid

The first investigation concerns the behaviour of the resonant frequency when the ferrite toroid dimensions are varied. An antenna operating

at a frequency range from 4 GHz to 5 GHz was designed following the procedure described in Section 3.1. The ferrite material used is the "Ferrite-3" type. The remaining space under the patch and beyond that, is occupied by the "RT 5870" dielectric. According to these characteristics, a geometry of patch radius $c = 5.8$ mm and inner ferrite radius $\alpha = 0.1 \cdot c = 0.58$ mm was estimated. The resonant frequency dependence is shown in Fig. 8 versus the ratio of ferrite toroid over the total patch dimension $(b - \alpha)/c$ for a constant DC magnetization $H_0 = 1375$ Oe and $\alpha/c = 0.1$, $b/c = 0.1$ to 0.9. The curves for a lossless ferrite material are also presented in the same graph along with a comparison against HFSS simulations. The resonance curves for the lossy ferrite case vanish as they approach the vicinity where μ_{eff} becomes negative. This is also confirmed by the HFSS results.

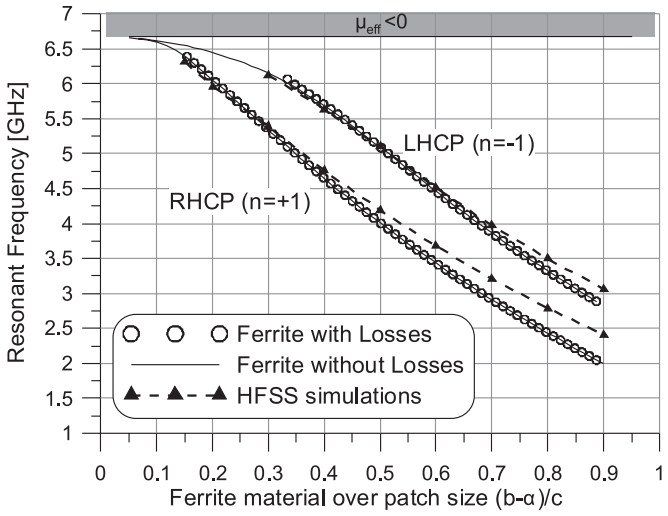

Figure 8. Resonant frequency of a circular patch antenna of radius c tuned by a ferrite toroid ($\alpha < \rho < b$) versus the normalized ferrite dimensions $(b - \alpha)/c$.

Figure 9 presents the resonant curves of a circular patch of radius $c = 7.5$ mm and $\alpha = 0.75$ mm tuned by a "Ferrite-3" toroid type versus DC magnetization. All the other geometrical characteristics are the same as for the previous example. Only the lossy ferrite curves are shown in this graph. The excitation of an LHCP mode inside the negative μ_{eff} region is clearly observed in this case as well. Moreover, it is important to note that near the lower negative μ_{eff} asymptote, only a finite number of modes is excited. An infinite number of curves would be expected if ferrite losses were not taken into account.

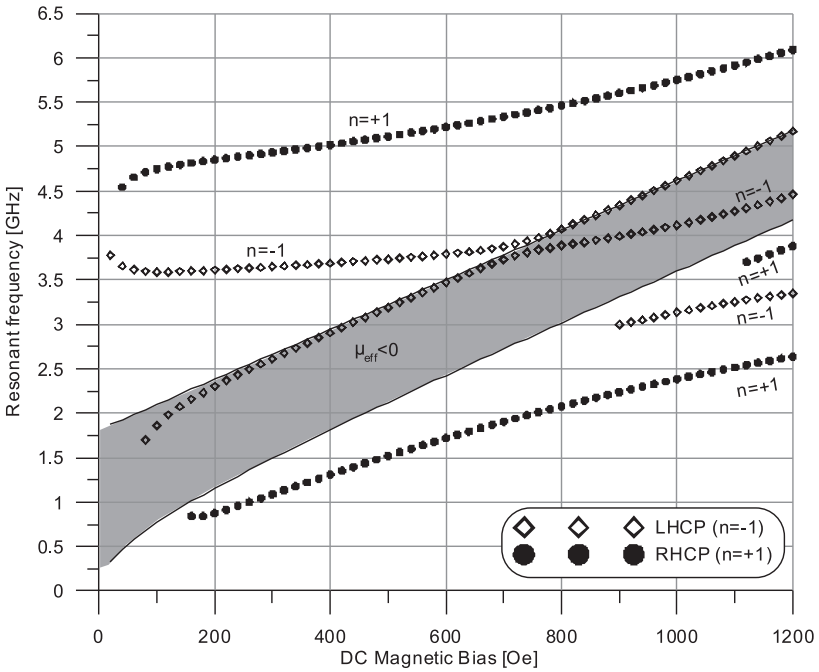

Figure 9. Resonant frequency of circular patch ($c = 7.5\,\text{mm}$) tuned by a ferrite toroid (Ferrite-1, $\alpha = 0.1 \cdot c$, $b = 0.8 \cdot c$) versus DC magnetization ($\overline{H}_{DC} = H_0 \widehat{z}$).

4.5. Electronic Tuning

The numerical results for the electronic tuning shown in above examples is summarized in Table 3 for the first $RHCP_1$ and the second $LHCP_2$ mode (resonating within $\mu_{eff} < 0$). The $RHCP_1$ always presents higher tuning sensitivity, but the $LHCP_2$ could be preferable for its unique features.

4.6. Results for the Input Impedance

The input impedance is a very important characteristic since it defines the antenna bandwidth. So, it is useful to investigate the input impedance behaviour of the patch geometries studied in the previous sections. For this purpose numerical simulations employing the Ansoft HFSS are carried out, throughout the frequency tuning range. A significant variation of the resonant impedance versus tuning is observed for a specific fixed feeding position. For an optimum antenna

Table 3. Electronic tuning, dynamic range and sensitivity for the first $RHCP_1$ and the second $LHCP_2$ mode (inside $\mu_{eff} < 0$).

Patch Geometry	Polarization $n = \pm 1$	f_{min} (GHz)	f_{max} (GHz)	Dynamic Range		DC-bias ΔH_0	Tuning Sensitivity
				Δf(MHz)	Δf(%)	(Oe)	(Mhz/Oe)
Ferrite	$RHCP_1$	0.1	2.4	2300	184%	1180	1.95
Substrate	$LHCP_2$	3.7	4.6	900	22%	540	1.7
Ferrite	$RHCP_1$	0.7	2.8	2100	120%	1180	1.8
Post	$LHCP_2$	3.55	3.75	200	5.5%	400	0.5
Ferrite	$RHCP_1$	0.3	2.6	2300	158%	1180	1.9
Toroid	$LHCP_2$	3.7	4.4	700	17%	500	1.4

efficiency a matching network following/compensating this variation should be incorporated. This can be achieved using an appropriate printed circuit. For further elaboration on wideband matching the reader can refer to classical circuit synthesis handbooks, e.g., [17].

The input impedance versus frequency with H_{DC} as a parameter for a circular patch printed on a ferrite substrate is shown in Fig. 10. The geometry is the same as that of Fig. 4. The results concern the first RHCP mode and originate from numerical simulations performed with Ansoft HFSS software. The antenna is excited by a coaxial probe at an offset position $\rho = 4.9\,\text{mm}$ with a characteristic impedance of 50Ω. The resonant input resistance is equal to 50Ω (matching) for $H_0 = 800\,\text{Oe}$ and varies from 35Ω to 90Ω as H_{DC} varies from 600–1100 Oe.

A similar graph is presented in Fig. 11 for the case of a circular patch tuned by a ferrite post. The patch radius is b=12mm while the post radius to patch ratio is kept constant to $\alpha/b = 0.5$. The ferrite and dielectric characteristics are the same as for the antenna of Fig. 7. The coaxial probe was placed at an offset $\rho = 7\,\text{mm}$ inside the dielectric material region. This was done on purpose, in order to avoid drilling the ferrite material, which is quite a difficult task in practice. This feeding position leads to a resonant resistance of 50Ω (matched) at $H_0 = 600\,\text{Oe}$ and varies from 30Ω to 80Ω as H_{DC} changes from 400–900 Oe.

The graph of Fig. 12 shows the resonant resistance as a function of H_{DC} for the case of a circular patch tuned by a ferrite toroid. The patch dimensions are the same as in the case presented in Fig. 9. The

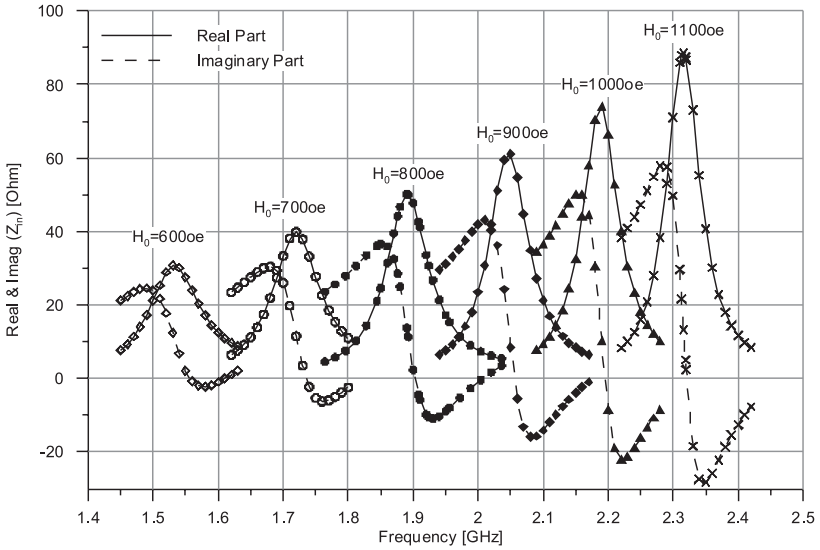

Figure 10. Input impedance of the first RHCP mode versus frequency with H_{DC} as a variable for the circular patch antenna studied in Fig. 4.

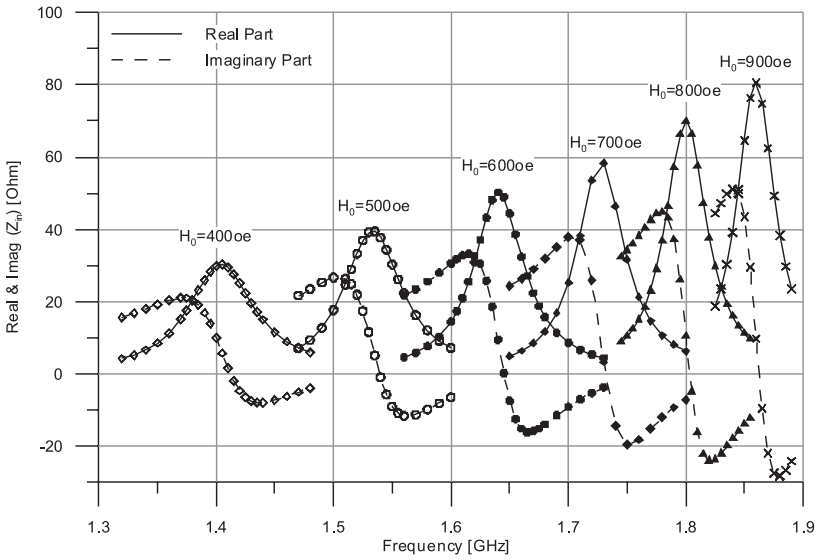

Figure 11. Input impedance of the first RHCP mode versus frequency with DC magnetization as a variable for a patch tuned by a ferrite post, for a case presented in Fig. 7.

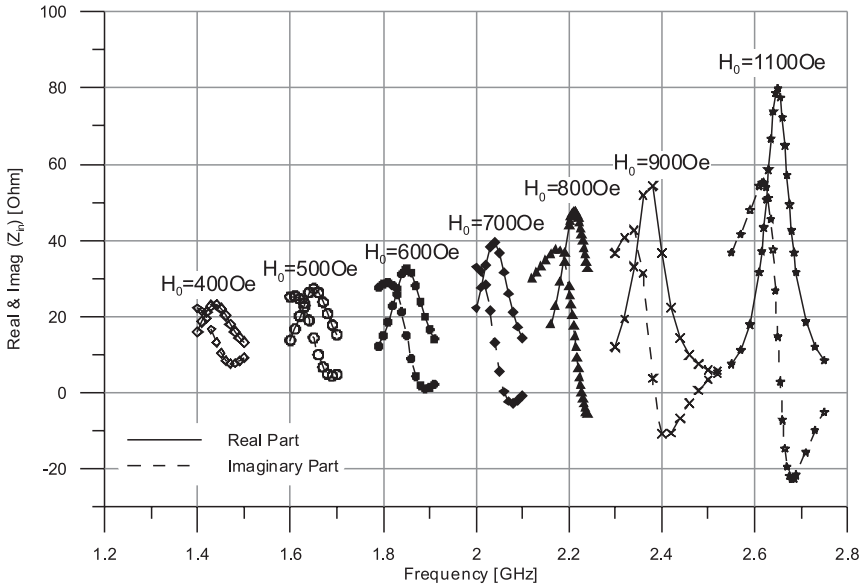

Figure 12. Input impedance of the first resonant RHCP mode versus frequency with DC magnetization as a variable for a patch tuned by a ferrite toroid.

probe feed position is at an offset $\rho = 4.5\,\text{mm}$. In the present case it was difficult to achieve matching because the area filled with dielectric is either near the center of the patch which gives a low value for the resonant resistance or near the edge of the patch which leads to a high value. For the selected probe position the resonant resistance is equal to 50Ω (matching) for $H_0 = 800\,\text{Oe}$ and varies from 23Ω to 80Ω as H_{DC} changes from 400–1100 Oe.

Fig. 13 concerns the same geometry as in Fig. 12, only now the input impedance of the second LHCP mode excited inside the negative μ_{eff} region is shown. The feeding probe is placed at a new offset position $\rho = 4.6\,\text{mm}$ offering an input impedance of $50\,\Omega$ (matching) at DC magnetization $H_0 = 1000\,\text{Oe}$.

Since all patch antennas behave as effective radiators around their resonant frequency, it is then very useful to summarize the corresponding results of Figs. 10, 11, 12 and 13. For this purpose the resonant resistance versus DC magnetization is shown in Fig. 14. The matching to the coaxial feed is marked with circular marks.

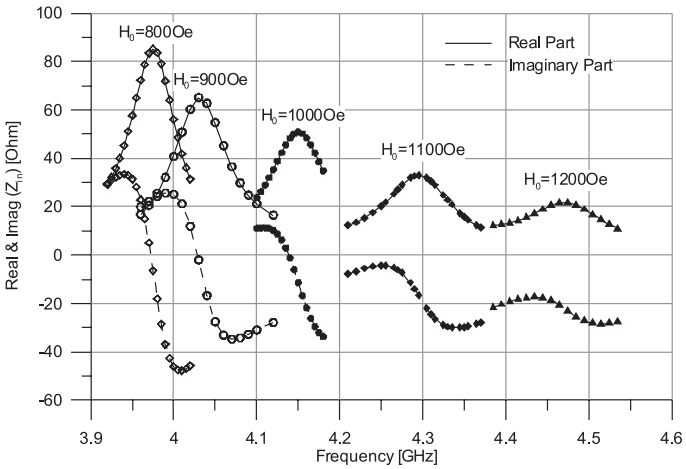

Figure 13. Input impedance of the second LHCP mode (inside the $\mu_{eff} < 0$ region) versus frequency with DC magnetization as a variable for the same geometry as in Fig. 12.

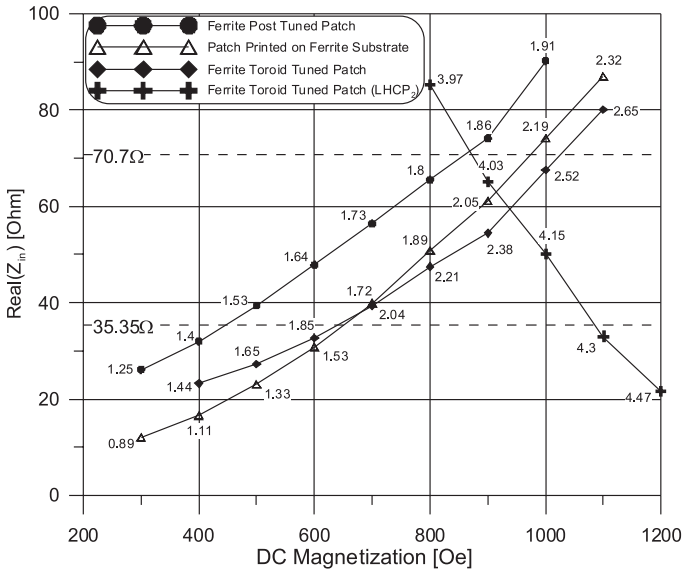

Figure 14. Input impedance versus DC magnetization for a patch printed on a ferrite substrate, a patch tuned by a ferrite post and a patch tuned by a ferrite toroid. The numbers next to the markers denote the resonant frequency (in GHz) of the mode at the corresponding DC magnetization value.

5. CONCLUSIONS

The resonant characteristics for a number of different circularly symmetric patch antennas tuned by transversely magnetized ferrite were presented. The electronic tuning of the right and left hand circular polarizations was extensively studied for saturated bulk as well as post or toroid ferrite tuning. A novel LHCP mode propagating inside the negative μ_{eff} region was found. In all cases the patch antennas were found to resonate at this mode and their resonance frequency and input impedance was studied. Taking ferrite magnetic losses into account proved essential since it explained better the behaviour of modes excited on the borders of the negative μ_{eff} region. Dielectric losses of the materials involved (including ferrite) are also included in the analysis and simulations. Furthermore, the partially magnetized ferrite state was studied employing the corresponding ferrite permeability tensor. The "perfect magnetic walls" approximation was employed in order to get a physical insight and to establish a design procedure. The calculated results were found in good agreement with experimental results published in the literature and with simulations performed with commercially available software.

REFERENCES

1. Cadieu, F. J., "High coercive field and large remanent moment magnetic films with special anisotropies," *J. Appl. Phys.*, Vol. 61, 4105–4110, 1987.
2. Mavridis, A. A., G. A. Kyriacou, J. N. Sahalos, "Analysis of circular patch antenna tuned by a ferrite post," *Microwave & Optical Technology Letters*, Vol. 46, No. 3, 234–237, Wiley, Aug. 5, 2005.
3. Pozar, D. M., "Radiation scattering characteristics of microstrip antennas on normally biased ferrite substrates," *IEEE Trans. AP*, Vol. 40, No. 9, 1084–1092, Sep. 1992.
4. Baccarelli, P., C. Di Nalo, F. Frezza, and P. Lampariello, "Anomalous propagation, loss and radiation effects in open waveguides with gyrotropic media," *IEEE MTT-S Digest*, Vol. 1, 283–286, 17–21 June 1996.
5. Baden-Fuller, A. J., *Ferrite at Microwave Frequencies*, IEE Publishing, 1987.
6. Pozar, D. M., *Microwave Engineering*, Third Edition, Wiley, 2005.
7. Lewin, L., *Theory of Waveguides*, Newnes-Butterworths, 1975.
8. Kyriacou, G. A., A. A. Mavridis, and J. N. Sahalos, "Approximate

resonant frequencies of certain antennas printed on magnetized ferrite," *URSI Int. Symp. on Electromagnetic Theory*, 97, Toronto-Canada, Aug. 13–21, 1999.

9. Waldron, R. A., *Ferrites: An Introduction for Microwave Engineers*, D. Van-Nostrand, 1961.
10. Batchelor, J. C., G. Classen, and R. J. Langley, "Microstrip antennas on ferrites," *10th Int. Conference on Antennas and Propagation*, April 14–17, 1997, Conference Publication No. 436 ©IEE, 1997.
11. Tsang, K. and R. J. Langley, "Annular ring microstrip antennas on biased ferrite substrates," *Electronics Letters*, Vol. 30, No. 16, 1257–1258, Aug. 4, 1994.
12. Green, J. J. and F. Sandy, "Microwave characterization of partially magnetized ferrites," *IEEE Trans. MTT*, Vol. MTT-22, No. 6, June 1974.
13. Mavridis, A. A., G. A. Kyriacou, S. Diamantis, and J. N. Sahalos, "On the design of dynamically controlled patch antennas printed on magnetized ferrite substrates for communication applications," *COMCON8*, Rythimna, Greece, June 25–29, 2001.
14. Bahl, I. J. and P. Bhartia, *Microstrip Antennas*, Artech House, Ottawa, 1980.
15. Araki, K., D. I. Kim, and Y. Naito, "A study on circular disk resonators on a ferrite substrate," *IEEE Trans MTT*, Vol. MTT-30, No. 2, 147–154, February 1982.
16. Ansoft, *HFSS version 8.0.21*, Ansoft Corporation, copyright 1984-2001.
17. Matthaei, G., E. M. T. Jones, and L. Young, *Microwave Filters, Impedance-Matching Networks and Coupling Structures*, Artech House, 1980.